Deep Separable Convolution Network for Prediction of Lung Diseases from X-rays

Geetha. N[1]

(Reg No. BDU2120412778980) Research Scholar in Computer Science, J.J college of Arts and Science (Autonomous), Sivapuram Post, Pudukkottai (Affiliated to Bharathidasan University, Tiruchirapalli)
Tamil Nadu, India

Dr. S. J. Sathish Aaron Joseph S. J[2]

Assistant Professor and Research Advisor in Computer Science, (Ref.No:05526/Ph.D.K 10/Dir/Computer Science/R.A), P.G and Department of Computer Science J.J.College of Arts and Science (Autonomous)
Sivapuram, Pudukkottai, Tamil Nadu, India

Abstract—Accurate diagnosis of lung cancer has been critical, and image segmentation and deep learning (DL) techniques have made it easier for medical people. Yet, the concept's effectiveness is extremely limited due to a scarcity of skilled radiologists. Although emerging DL-based methods frequently necessitate accordance with the regulation, such as labelled feature map, to train such networks, which is difficult to terminate on a big scale. This study proposed a swarm intelligence based modified DL model called MSCOA-DSCN to classify and forecast various Lung Diseases through anterior X-rays. Image enhancement with a modified median filter and edge enhancement with statistical range applied for better image production. The disparity between min and max pixels focused on the Statistical range from each 3×3 input image cluster. Utilized Enriched Auto-Seed Fuzzy Means Morphological Clustering for segmentation (EASFMC); they could function together to identify edges in X-Ray imaging. Used A deep separable convolution network (DSCN) was in the created system to predict the class of lung cancer, and Modified Butterfly Optimization Algorithm (MBOA) applied for the feature selection procedure. This present study compared with various state-of-the-art classification algorithms using the NIH Chest-Xray-14 database.

Keywords—*Lung diseases; X-rays; deep learning; filtering; edge detection; segmentation and swarm intelligence*

I. INTRODUCTION

In recent times, Lung cancer (LC) is the main leading causes of mortality among the most dangerous tumours that can harm a person's health. It has the highest mortality rate, including all tumours, and is the prominent basis of cancer death in human [1]. LC accounts for roughly 1.8 million people infected each year, or 13% of all cancer cases, and 1.6 million fatalities globally, or 19.4% of all cancer-related deaths. In 2020, the expected mortality of cancer patients in developing countries [2] was 679,421 men and 712,758 females, particularly in India. Around one in 68 men suffers this form of LC; about one in 29 women suffer breast cancer, therefore around one in nine Indians suffering cancer between the decades of 0 and 74.Increasing the risk of LC, the discovery in the early stages will improve survival rates significantly. Still, it is also impossible to discern the early-stage prediction of LC due to fewer symptoms [3].

Computer-based technology has significantly grown in importance around the globe. As of early January 2019, COVID-19 causes causing substantial respiratory problems and severe health issues, leading to the possibility of the COVID-19 pathogenic virus and other such bacterial or viral infections [4]. As a result, the accurate intervention of lung disorders is rather critical than ever. Machine learning (ML) and DL can be beneficial throughout this case. The recognition of medical images in ML-based detection approaches necessitates a specific stage to isolate malignancies, automatic localization, and identification in internal organs, as well as particular processing, which is highly useful [5]. "DL approaches" that perform well in cancer categorization advance current trends.

Various studies have focused on how DL schemes might be used [6,7] with both the expansion of computer programming for medicine and social research initiatives, this approach has the potential to lower medical expenditures. The NIH chest X-ray image database is obtained mainly from the Kaggle repository [8] for use in development. A number of research works have been carried out on the diagnosis of chest diseases using artificial intelligence methodologies. In [9], multilayer, probabilistic, learning vector quantization, and generalized regression neural networks have been used for diagnosis chest diseases. The diagnosis of chronic obstructive pulmonary and pneumonia diseases was implemented using neural networks and artificial immune system [10]. In [11], the detection of lung diseases such as TB, pneumonia, and lung cancer using chest radiographs is considered. The histogram equalization in image segmentation was applied for image preprocessing, and feed forward neural network is used for classification purpose. The above research works have been efficiently used in classifying medical diseases; however, their performance was not as efficient as the deep networks in terms of accuracy, computation time, and minimum square error achieved. Deep learning-based systems have been applied to increase the accuracy of image classification [12]. These deep networks showed superhuman accuracies in performing such tasks. This success motivated the researchers to apply these networks to medical images for diseases classification tasks, and the results showed that deep networks can efficiently extract useful features that distinguish different classes of images [13]. Most commonly used deep learning architecture is the convolutional neural network (CNN). CNN has been applied to various medical images classification due to its power of extracting different level features from images

[14] [15]. This work presents a novel hybrid method for classifying lung illness in the aforementioned dataset. The research's significant contribution is the invention of a different hybrid DL system appropriate for detecting lung illness from X-ray pictures.

The study discusses the architectures of DSCN further with MBOA to help determine whether use individuals to diagnose LC in this research would work. The NIH chest X-ray image database is initially pre-processed images after that trained using the suggested DSCN-MBOA model to assess the percentage of lungs directly impacted by cancer and network image preparedness for LC. The networks in this translucent classification structure have achieved equivalent performance, latency (time), recall, f-measure, precision, and accuracy metrics. The following is the work's main contribution:

- The input x-ray images are first pre-processed with a modified median filter for noise reduction and statistical range edge detection.

- Enriched Auto-Seed Fuzzy Means Morphological Clustering is used for segmentation (EASFMC).

- By using DSCN and the MBOA for feature selection, the created method identifies a certain kind of lung illness.

The following is a conceivable structure for the manuscript: The second section discusses relevant research on lung classification and nodule identification and classification. Section 3 discusses the methodology of this study and a complete examination of the implemented dataset. Section 4 describes the findings and experimental discussion with their appropriate outcome results, while Section 5 finishes the research work with recommendations for further research.

II. RELATED WORK

A complete examination of numerous LC detection approaches for forecasting cancer is an uncontrolled development in the lung region, notably in lung X-ray images described in this literature review. Liu et al. [16] developed a Convolutional Neural Network (CNN)-based cascade technique for lesion classification. To get the localization of the focal liver lesions, initially utilize the transfer learning (TL) method to learn the automatic recognition network on the experimental dataset. Peng et al., [17] utilized a parallel genetic algorithm (GA) to detect LC in chest X-ray images. The approach combines pattern matching and localized search strategies, and experiments have shown promising outcomes.

The 121-layer CNN (DenseNet121) and the TL algorithm being investigated by Ausawalaithong et al., [18] are mechanisms for diagnosing LC via chest X-ray data. This classifier trained on the sample until moving on to the LC image database to overcome the difficulty of a short dataset. Yan et al. [19] suggested a weakly supervised DL architecture comprising squeeze-and-excitation blocks, multi-map transfer, and max-min pooling for grouping similar respiratory diseases, including identifying anomalous lesion locations on Chest X-ray14 dataset for diagnosing major lumbar spinal disorders. The extensive simulation shows that the proposed model has high effectiveness than the existing methods.

Yan et al. [20] described a new weakly-supervised learning model for classifying pulmonary diseases based on the analysis of given chest X-rays and localizing disease patches on X-rays at pixel-level refinement. The suggested network's benefits come from the acquisition of disease-specific characteristics during multi-map transfer layers and the cross-channel feature realignment provided by squeeze-and-excitation blocks somewhere between dense partitions. Heat maps, which are the raw material for producing the network's range of processes, are another way to display it.

The above X-ray scans are massive, containing 110,120 images and weighing almost 44 GB. Including the Chest X-ray-based LC expert systems, in [21] performed a thorough statistical study of different DL network models. The main objective is to obtain a performance evaluation for each DL network structure. It includes aspects of measurement, including accuracy performance, examination of training and validation time, memory utilization analysis, CPU and memory observation, graphics processing energy consumption, and some enhancement ideas.

In [22] suggested a Modified AlexNet (MAN) DL architecture to assess the lung abnormalities, where a threshold filter to reduce artifacts from Lung CT images is applied. Besides combining in-depth features with handcrafted features, this study introduces a new Ensemble-Feature-Technique (EFT). However, serial fusion and Principal Component Analysis (PCA)-based design to identify the significant feature set used. Compared to the other existing framework methods, experimental data show that MAN outperforms them. Bharati et al. [22] created new hybrid DL architecture (By merging data augmentation, VGG, and spatial transformer network (STN) into CNN) and denoted as VDSNet. Table I show the proposed methods' advantages and disadvantages in this literature review.

Here the Inference from the existing works is considered as conventional DL algorithms are robust, they underachieve when images are slanted, flipped or otherwise abnormally oriented. Again, hybrid approaches to evaluate the accuracy while reducing the learning rate are applied. The presented hybrid technique named DSCN- MSCOA may detect suspicious problematic regions using chest X-ray images that are highly effective and enhance diagnosis when compared to standard methods. In a way, it can improve the therapy's effectiveness for the affected individual in terms of accuracy, precision, etc.

TABLE I.   EXISTING PROPOSED METHODS WITH THEIR ADVANTAGES AND DISADVANTAGES

Author	Dataset	Method	Advantages	Disadvantages	Performance metrics
Liu et al., [9]	2594 chest x-rays and JSRT dataset	Cascaded CNN	Reduce the number of actions required to detect the condition and increase the learning duration.	The issue with using CNN to diagnose LC is that it is highly effective when the sample size is too small.	JSRT dataset: Precision of 0.885 and recall of 0.858 Chest x-ray: Precision of 0.985 and recall 0.958
Peng et al., [10]	154 pieces of medical images	GA	This results in more accurate learning without having to spend more time on it.	The reality that all tumor spots on chest X-rays were genetic conditions is overlooked because GA will not handle various diseases sequentially.	optimal solutions 100% execution time 14814s
Ausawalaithong et al., [11]	JSRT Dataset and ChestX-ray14 Dataset	CNN with TL	This suggested scheme is capable of resolving the issue of a small dataset.	Owing to the unavailability of features which include genetic factors and tobacco consumption rate in learning, as well as images, accuracy is reduced.	mean accuracy: 74.43±6.01%, mean specificity: 74.96±9.85%, and mean sensitivity: 74.68±15.33%
Yan et al., [13]	ChestX-ray14 dataset	weakly-supervised DL framework	As more of a result, using minimal samples can yield high accuracy.	Using the minimal number of bounding boxes, re-investigate an effective representation of lesion regions.	Average AUC 0.8302
Wibisono et al., [13]	110,120 images	five different CNN models	In terms of execution rate and accuracy, this might be the most efficient DL conceptual model.	The availability of sufficient labeling by a medical expert is a key barrier to applying DL models to serious health concerns.	AUROC scores 0.80 - 0.82, CPU utilization 527% - 940% memory usage 23.39 GB - 38 GB and execution time 2.91 hours - 7.6 hours.
Bhandary et al., [14]	chest X-Ray images and LIDC-IDRI	modified AlexNet	It is essential because it could be viewed as a program that helps physicians in doing further diagnostic procedures.	Though the recognition rate was improved by 0.05 on the ROC-AUC scoring system, there was always scope for change.	classification accuracy 97.27%
Bharati et al., [15]	NIH chest X-ray	VDSNet	It takes a lot less time to train, but the accuracy rate is significantly worse.	Unfortunately, this should result in a lengthy period of training.	validation accuracy of 73%

III. PROPOSED METHOD

An optimized DL-based technique opts to classify and extract LC regions on X-ray images. The proposed framework is composed of various successive components shown in Fig. 1. After pre-processing X-ray images using a modified median filter, the undesired LC components are masked using Enriched Auto-Seed Fuzzy Means Morphological Clustering (EASFMC) based segmentation and removal. After that, the features are extracted from the final fully-connected layers for the DSCN architecture, which are then optimized using MBOA. The optimized feature set input for DSCN for LC classification. Pre-processing is required because this technique requires an X-Ray image representation that could have noise, inappropriate blurring, or being out of perspective.

A. Dataset Description

The dataset [8] file comprises a random sample of 5% of the whole dataset, with 5606 photos with a resolution of 1024 x 1024 pixels each. To build a .csv (comma-separated values) file with patient data in addition class labels for the entire dataset. The following is a description of the class. There are 15 "No findings" classes, as well as 14 diseases such as Edema type images (118), Emphysema type images (127), Cardiomegaly type images (141), Fibrosis type images (84), Pneumothorax type images (271), Consolidation type images (226), Pleural Thickening type images (176), Mass type images (284), Effusion type images (644), Infiltration type images (967) and Nodule type images (313). Also, technique classifies "No finds" for 3044 images.
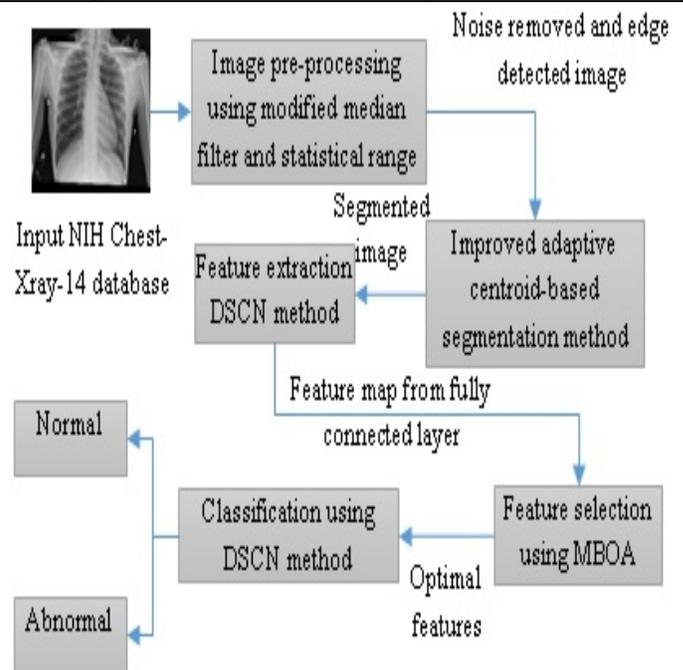
Fig. 1.   General Framework Diagram.

B. Image pre-processing and Edge Detection

Modified Median Filter for noise Removal: The median filter [23] is the most widely utilized image-enhancing filter. It blurs and distorts images by modifying noisy, denoted as

corrupted pixels, and noiseless, indicated as uncorrupted pixels. The modified median filters incorporate a switching mechanism to replace several pixels when it is determined to be contaminated. These results of pixels in an image are computed by Algorithm 1. A three × three window across the image stretches by starting in the upper left corner. Its function is associated with the maximum and minimum image pixels within the window to determine whether a pixel remains uncorrupted or corrupted. When a pixel's value is between the top and minimum, it is uncorrupted. A refined pixel is left alone within a specified filtering window, whereas corrupted pixels swap by the median image pixel or an effectively understood immediate adjacent pixel; is done for each pixel value. Determine the absolute value ϑ by the difference between both the window's centre pixel as well as its neighboring pixels with n=8, which is expressed as in Eq. (1-2):

$$\vartheta = \frac{\sum_{i=1}^{n}|\varphi(i,j)|}{n} \text{ where } i,j = 1,2,\dots,n \tag{1}$$

$$thershold = \mu\left[\frac{avg}{avg+var}\right] \tag{2}$$

where the $threshold$ is the ideal threshold in the proposed algorithm and is the mean of (i,j). In the filtering window, the mean avg, as well as variance var of n neighbor pixels nearest to the center pixel, as well as variance var of n neighbor points adjacent to the center pixel is determined. It can be explained simply:

$$var = \sqrt{\frac{\left(\sum_{i=1}^{n} x(i,j) - ave\right)^2}{n}} \text{ and } avg = \frac{\sum_{i=1}^{n} x(i,j)}{n} \tag{3}$$

Algorithm 1. The modified median filtering algorithm

Input: Corrupted Input chest X-ray Image by noise

Output: Noise removed Image, using a $M \times N$ window

1. The $M \times N$ window is skimmed in excess of the entire image.
2. Category the pixels, denoted by S_{ij} inside the window in ascending order.
3. Find minimum S_{min}, maximum S_{max} and median S_{med} of the pixel values
4. If ($S_{min} < S_{epicenter} < S_{max}$)
5. denote the medium pixel as uncorrupted such that no filtering required
6. Else
7. denote the medium pixel as corrupted
8. If ($S_{epicenter}$ is not an noise which is margin significance)
9. Substitute $S_{epicenter}$ through S_{med}
10. Else
11. Substitute $S_{epicenter}$ through $S_{i-1,j}$
12. End If
13. End If
14. Recurrence step 2 to 9 for the complete image and obtain noise removed image.

Statistical Range for Edge detection: The measures of dispersion between every maximum and minimum value of a specified collected data, matrix, or linear data in massive volumes of data, the variety can be used to detect edges. Every pixel is supplanted with a variety of grey values from the surrounding area. The variety also gives meaning to the mean, median, as well as mode, it can gain a piece of deeper knowledge through a variety of facts. In this study, the statistical range (SR) from each of the 3 × 3 matrix partitions from the lung input image was examined. The equation for determining SR is as follows:

$$SR = S_{med} - S_{min} \tag{4}$$

C. EASFMC for Segmentation

The lung segmentation technique is a prerequisite in classifying lung images and yet is essential for effective cancer diagnoses. Earlier, used Otsu's approach [24] to determine a global specified threshold, then image edge detection was employed to extract the bounding box of the image's centre, i.e., the malignancy location on an image. The region is segmented using regions of interest with an EASFMC clustering methodology, a density-based technique for detecting spontaneously generated clusters in more extensive coverage of large databases with imperfection. EASFMC additionally clusters sites only in high-density areas, whereas endpoints in specific areas are considered outliers or interference. So the amount of segments is determined dynamically.

Based on EASFMC, the study proposes a method for extracting the characteristic features of cancer areas. The fuzzy concept, commonly employed in the classification process, is being used here for segmentation—the given image segments into several clusters due to specific fuzzified data clusters by keeping their geometric placements—the measure of similarity of each pixel to the precedent cluster's centre value using the membership degree. The method has indeed been designed in this study to determine its initial centroids reference value on its own, making the segmentation procedure automatic. The EASFMC Segmentation steps are explained in detail as follows.

Step 1: The ROI I(x,y) was obtained initially, which comprises the cancer area and the ordinary location, two reference cluster numbers must be specified for this. Those two main clusters c were generated sequentially in an attempt to implement this segmentation quickly and easily.

$$c_1 = \frac{\sum\left(\sum_{m=1}^{i} \max(I(m,:))\right)}{N}$$

$$c_2 = \frac{\sum\left(\sum_{n=1}^{j} \max(I(m,:))\right)}{N}$$

Where $m = 1,2,\dots,i$ and $n = 1,2,\dots,j$. $\tag{5}$

Where i is the amount of rows, j is the amount of columns in image $I(m,n)$ and N is the complete number of non-zero pixels.

Step 2: The differentiation between each pixel as well as clusters was computed, therefore two distance matrices, $dist_1$ and $dist_2$, respectively built for both c_1 and c_2 using the formulae below.

$$dist_1 = [c_1 - I(m,n)]^2 \text{ and}$$

$$dist_2 = [c_2 - I(m,n)]^2 \tag{6}$$

Step 3: The distance matrices acquired in the initial state were smooth fuzzified using the following equations, and even the coefficients were therefore normalised as well as fuzzified using a constant variable $\mathbb{r} > 1$ as then their summation was 1, as well as the resultant smooth fuzzified output was preserved in F_1 and F_2.

$$F_1 = \frac{1}{(dist_1)^{\frac{2}{\mathbb{r}-1}}} \text{ and}$$

$$F_2 = \frac{1}{(dist_2)^{\frac{2}{\mathbb{r}-1}}} \tag{7}$$

This seems to be comparable to simply normalising the coefficients to achieve their summation 1 for $\mathbb{r} = 2$.

Step 4: Around an image $F(m,n)$, fuzzy rule-based assignment was conducted prior to F_1 and F_2, as well as the segmented images seg_1 (the segmented image with respect to initial cluster c_1) and seg_2 (another segmented image with respect to cluster c_2) were generated as follows:

$$seg_1(i,j) = I(m,n), if\ F_2(i,j) < F_1(m,n) \text{and}$$

$$seg_2(i,j) = I(m,n), if\ F_2(m,n) > F_1(m,n) \tag{8}$$

Step 5: The seg_1 and seg_2 were refined through updating the cluster value c_1 and c_2 consuming the subsequent equations.

$$c_{1update} = \frac{\sum(seg_1(i,j)\neq 0)}{N_1} \text{ and}$$

$$c_{2update} = \frac{\sum(seg_2(i,j)\neq 0)}{N_2} \tag{9}$$

Where N_1 and N_2 are the complete amount of non-zero pixels in seg_1 and seg_2 correspondingly.

Step 6: Step 1 to 5 were repetitive once more with the new cluster centre values such as $c_{1update}$ and $c_{2update}$ up to the difference between two sequential restructured clusters were minimum.

Step 7: Mathematical morphology is used for the binary image, and the cancer regions are improved in the processed binary image. Formerly, DSCNN is applied for feature extraction yields the final results of feature extraction then also classification after X-ray image segmentation.

D. Feature Extraction and Classification using DSCNN

In DSCNN, image features are extracted from the fully connected (FC) layers and then optimized utilizing the MSCOA method. The system gave a 2-dimensional feature map containing the retrieved image features as input. Provide N filters to every convolutional network layer to identify cancer region abnormalities across data points. Every neural inference produced a probability function in maintaining the likelihood of every output class. Fig. 3 depicts the DSCNN classifier's architectural framework. The network's initial layer was a normal convolutional layer throughout all situations. Another batch-normalization layer including activation function (rectified linear unit (ReLU) [25]) followed the convolutional layer.
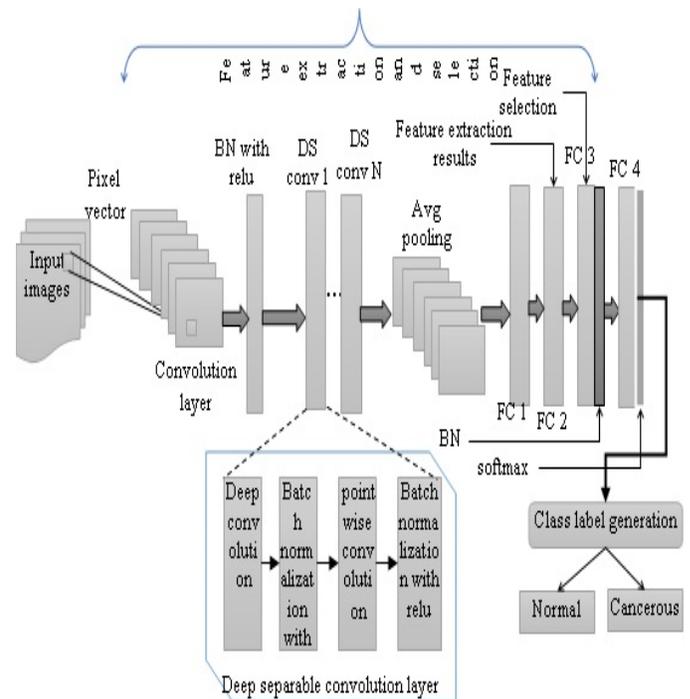
Fig. 2. General Architecture of the DSCNN for LC Detection.

Sophisticated features are represented efficiently by DSCNNs. Meanwhile, the number of convolution layers (Conv) and its type, pooling function, kernel size and activation function, and fully connected layers model. The primary goal is to acquire outstanding raw pixel information to identify the detection efficiency of the overall architecture. Following the DSCNN process of learning, MSCOA is used to isolate the optimal feature selection, just the most essential attributes that maximize classification performance. The DSCNNs fundamental aim of sharing weights over multiple layers is to reduce the curse of dimensionality. Can summarize entire network as (Conv1: $1 \times 3@64$) $\rightarrow$ (DSConv2: $1 \times 3@64$) $\rightarrow$ (FC1: 128) $\rightarrow$ (FC2: 128) $\rightarrow$ (FC3: 64) $\rightarrow$ (BN: 64) $\rightarrow$ (FC4: 64) and Fig. 2 shows the suggested DSCNN architecture into four layers: (1) Conv (2) Deep Separable Convolution layer (DS Conv), (3) Pooling layers, and (4) FC.

Conv: This is the first conv, with 64 filters, a kernel of dimension 3, as well as a stride of value 1, and it employs the ReLU as a non-linear function, followed by dropout regularization with a rate of 0.5 and then a size two max-pooling operations.

DS Conv: This is the second DS Conv, similar to Conv1, except that instead of max-pooling, this uses an adaptive average pooling layer.

FC: FC1, FC2, and FC3 are feature extraction and feature selection layers that output learned features from raw input, with 128, 128, and 64 neurons.

BN and FC4: FC4 is the final FC layer to produce the classification predictions, and BN (batch normalization) operation.

BN was used to speed up the training process while also reducing the risk of overloading due to regularization. After BN and ReLU activations, the input image array to the first conv layer. each of the DS conv layers 1 to N starts with a deep convolution, then BN and ReLU, before moving on to a pointwise conv, BN, and ReLU activation again. The application determines average pooling and FC layer containing soft max activations after the conv layers. Great learning rates can be employed when the activation patterns since the strength of the biases of each layer are much more equivalent, resulting in rapid system divergence.

The small number of features in the mini-batch creates a regularization effect since the activations of a single image file are not normalized by the mean and variance of each image file but rather by the mean and variance of the mini-batch wherein it occurs. Following the BN layer, a series of DS convs consisted of a deep wavelet convolution (DW conv) and a pointwise convolution (PW conv). A BN followed each one with ReLU activation. After that, an average pooling layer decreases the number of activations by introducing an averaging window to every input cable network's complete time-frequency feature map. Finally, the probabilities for every class label using an FC layer with softmax activations.

E. Feature Selection using MBOA

The food gathering behavior of butterflies [26] inspired the Butterfly Optimization Algorithm (BOA) used to find and identify the best solution in a multi-dimensional domain. To reach a local and global optimum solution, certain unique places are allocated to butterflies in the ecosystem, including some input values. The calibration period starts after this, and the method runs like a virtual environment, optimizing the location of the features (butterflies) by tweaking its parameter. The primary three variables of the butterfly algorithm are used to move features (butterflies) from its random position to the optimal solution whereas butterflies use their keen sense of smell and scent to detect the presence of other butterflies.

Each scent in BOA has its unique distinct, enticing aroma and unique touch. This is one of the guiding features that set BOA apart from other meta-heuristics. To understand how fragrance is regulated in BOA [26], first understand how a technology such as music, lighting, or warmth is computed. The entire concept of identifying and managing the method is based on three key terms: stimulus intensity ($\mathcal{I}$), power exponent ($\mathcal{E}$) and sensory modality ($\mathcal{M}$). Sensation implies measuring the variety of energy and processing it by comparing methods in sensory modality technique, while methodology implies the basic information used by the sensors.

Currently, numerous modalities include lighting, music, and warmth. In BOA, while sI is the strength of the physical stimulus, when a butterfly emits a more visible smell, other butterflies in the area can sense be drawn towards it. The power of the butterfly or rational response represents an improvement in intensity, where pE is the parameter that

considers regular expression, which accounts for fluctuating levels of absorption. This part conducted several stimuli estimating experiments on bugs, critters, and individuals, and they have hypothesized that as the number increases, insects become less sensitive to changes in the environment. Using these ideas, the fragrance $\mathfrak{FR}_i$ (fragrance is smell by i th butterfly) in BOA is computed as [27]:

$$\mathfrak{FR} = \mathcal{M} * \mathcal{I}^{\mathcal{E}} \tag{10}$$

The global and the local search stage are utilized to assert that fragrance levels rise in a well-liked situation. A butterflies B would produce a smell that may be sensed from every location in the region in this manner. The butterfly finds the fitness values $\mathcal{F}$, which can be depicted as in the global search stage.

$$x_i^{iter+1} = x_i^{iter} + (\mathcal{R}^2 \times \mathcal{F} - x_i^{iter}) \times \mathfrak{FR}_i \tag{11}$$

where x_i^{iter} is the way out vector x_i for ith butterfly in iteration number $iter$. Fragrance of ith butterfly is represented by $frag_i$ and $\mathcal{R}$ is a random number which would be in between 0 and 1, also here $\mathcal{R} < P$, where $\mathcal{P}$ is the switching probability. Neighborhood or local search stage can be represented as

$$x_i^{iter+1} = x_i^{iter} + (\mathcal{R}^2 \times x_j^{iter} - x_k^{iter}) \times \mathfrak{FR}_i \tag{12}$$

where x_j^{iter} and x_k^{iter} are jth and kth butterflies from the search space. On the off chance that x_k^{iter} has a place with a similar swarm and x_i^{iter+1} turns into a neighborhood random walk. Scan for nourishment and mating accomplice by butterflies can happen at both neighborhood and global level and thus $\mathcal{P}$ is utilized as a part of BOA to switch between normal globe searches to concentrate local search.

By researching the scent and separating it from the poor one, the DSCNN-based feature findings contribute in the examination of fragrance in the movement of numerous butterflies and the transmittance of smell to interact to each other and go beyond the optimal butterfly. A butterfly with a little more fragrance and a higher fitness value can attract more butterflies in that region, and a butterfly with plenty of fragrance and sometimes a based on the fitness value can attract more butterflies in that area. Particles in the region can compress their replies by using the parameter $\mathcal{E}$. The $\mathfrak{FR}$ and $\mathcal{I}$ are the main issues to get the variance of $\mathcal{I}$ and formulation of $\mathfrak{FR}$. The values of $\mathcal{I}$ which are encoded with objective function and $\mathfrak{FR}$ is relative which is calculated as

$$\mathfrak{FR} = \mathcal{M} * \mathcal{I}^{\mathcal{E}} \left(1 - \frac{N_{tf} - N_{fs}}{N_{tf}}\right) \tag{13}$$

The accuracy of the DSCNN classifier has been employed as an efficiency analyzer in the creation of objective functions with a large number of features. Where (N_{tf}) denotes the overall quantity of features (tf), (N_{fs}) denotes the dimension of the feature subset (fs). The BOA's Sensory Modality $\mathcal{M}$ parameter instructs the butterflies to sense the fragrance

generated from other butterflies within the search region and direct their search to those providing the most scent [23]. Like the value of the $\mathcal{M}$, the parameter is increased, and the algorithm's performance improves throughout execution. As the number of iterations increases, the algorithm's performance improves for the period of the iterative search process. A significant impact on the efficiency of BOA and the performance will be enhanced considerably in comparison to the conventional BOA with Eq. (14), it is analyzed that the new values of $\mathcal{M}$ will have.

$$\mathcal{M}^{iter} = \mathcal{M}^{iter-1} * \frac{\left(10.0 - \frac{5}{0.9}\right)^2}{MaxGen} \tag{14}$$

where $iter$ is the current iteration number and MaxGen is the maximum number of iteration in the algorithm. In this suggested work, the adaptive mechanism of M is designed and used in the algorithm, which adds useful elements to the algorithm's performance and aids in acquiring alternative discoveries in the search space, enabling the BOA approach to achieve better results. The flowchart of MBOA is given in Fig. 3 and the pseudo code of MBOA is clarified in Algorithm 1.
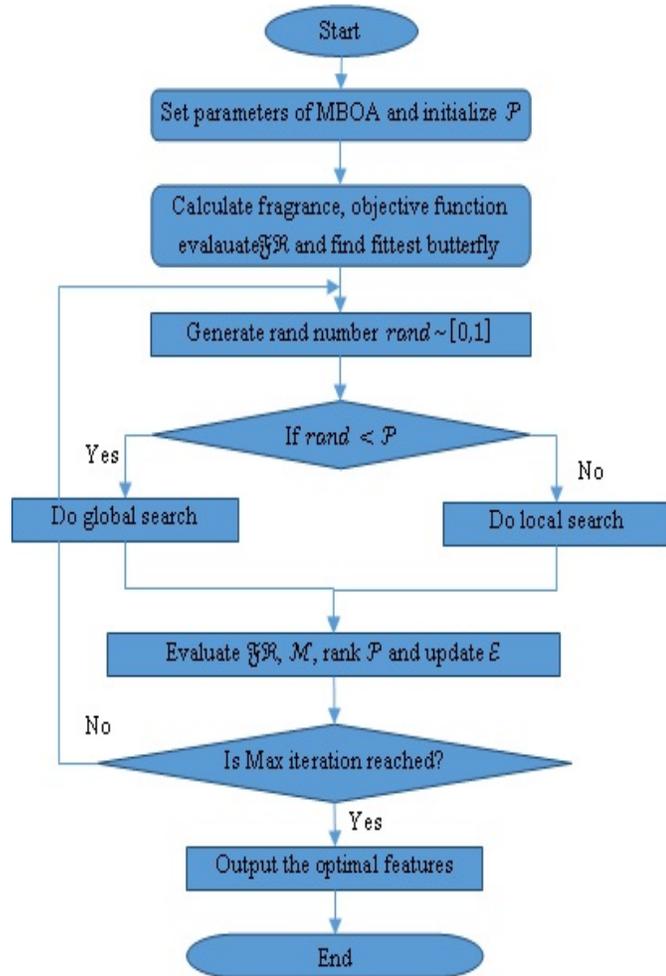
Fig. 3. Flowchart of Proposed MBOA based Optimal Feature Selection.

Algorithm 2. Pseudo-Code for MBOA for optimal feature selection

Input: Features extracted by DSCNN

Output: Feature subset selection (optimal features)

Begin
Do initial population of N butterflies $x_i = (i = 1, 2, \ldots, n)$
Determine$\mathcal{I}$ at x_i is determined by $\mathfrak{FR}(x_i)$
Outline$\mathcal{M}$, $\mathcal{E}$ and $\mathcal{P}$
while ending criteria not encountered do
for each butterfly in population do
Determine$\mathfrak{FR}$for butterfly using Eq. (10)
end for
Discover the paramount$\mathcal{F}$
ensure for each butterfly in population
Derive a random number $rand$ from [0, 1]
if $rand < \mathcal{P}$
Interchange in the direction of best solution using Eq. (12)
else
Interchange arbitrarily using Eq. (13)
end if
end for
Apprise the worth of $\mathcal{M}$
end while
while ending criteria reached do
Determine objective function (accuracy of the test set by DSCNN classifier) of butterflies are evaluated depend on Eq. (15);
return optimal butterflies (the selected optimal feature subset);
End while
End

IV. EXPERIMENTAL RESULTS AND DISCUSSION

The proposed work DSCNN-MBOA classifies the collected features into two class labels: normal and cancerous. The lung X-ray images are generally contained the noise, so, the first step of the work is applying pre-processing techniques to remove unwanted and noisy information for further analysis. After that, these images will be passed via an operation of segmentation in which the cancer region is extracted. Then the segmented image will be the given input of the proposed DSCNN-MBOA for detection of the LC, MBOA used for feature selection and various parameters are then utilized to assess the performance of the proposal such as accuracy, precision, F1-score, execution time, specificity and sensitivity and compare with exiting methods such as VDSNet [22], modified AlexNet [21] and CNN with TL [20].

$$Accuracy = \frac{TP+TN}{TP+TN+FP+FN} * 100 \tag{15}$$

$$Precision = \frac{TP}{TP+FP} * 100 \tag{16}$$

$$F1\ score = \frac{2*Precision*Recall}{Precision+Recall} \tag{17}$$

$$Specificity = \frac{TN}{TN+FP} * 100 \tag{18}$$

$$Sensitivity = \frac{TP}{TP+FN} * 100 \tag{19}$$

Here, FP described as False Positive, which is the total number of lung images that are presently negative and classified as positive. Where TP described as True Positive, which is the total number of lung images that are currently positive and classified as cancerous, FN described as False Negative, which is the total number of lung images that are presently positive and classified to be harmful as normal. TN described as True Negative, which is the total number of lung images that are currently negative and classified to be negative.

A. Accuracy Comparison Results

Fig. 4 gives the accuracy of proposed and existing models for the number of features in a shared database. The proposed DSCNN-MBOA increases the accuracy with a value of 98.45%. The reason for this is that the threshold is primarily used to alter the size of the sub training dataset, but it is also utilized for other purposes. The lower the value, the more likely the raw dataset samples are dispersed among the sub training datasets. The incorporation of the MBOA mechanism in the proposed model improves accuracy performance because it increases the convergence speed of DSCNN.

B. Precision Comparison Results

Fig. 5 indicates the precision of proposed and existing models for the number of features in a given database. As increasing the number of features, the precision is also maximized. E.g., the DSCNN-MBOA attains a precision of 98.5% compared to the VDSNet, modified AlexNet and CNN with TL. Because the DSCNN-MBOA combines feature extraction and classification into a single DSCNN-MBOA structure, it decreases the time necessary to compute the derived factors, resulting in a higher precision rate. DSCNN-MBOA performs best with high-speed converges, which is likely due to a lack of data on the features of the huge images, speeding up convergence time over the entire dataset.
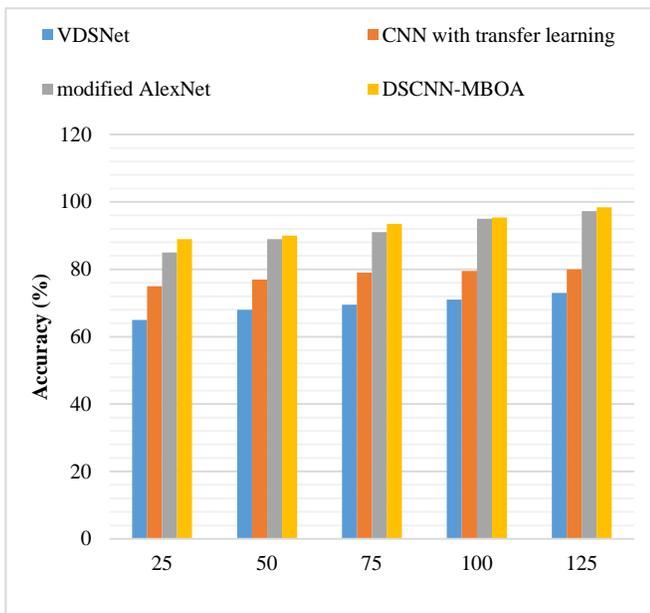
Fig. 4.   Accuracy Performance Comparison.
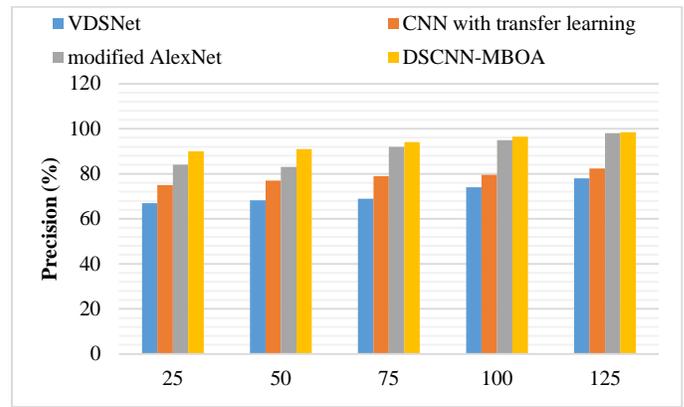
Fig. 5.   Precision Performance Comparison.

1) F1-sore comparison results: From Fig. 6, it indicates the F1-sore of proposed and existing models for the number of features in given databases. E.g., the DSCNN-MBOA provides an f-measure of 98.85% compared to all other models such as VDSNet, modified AlexNet and CNN with TL. The reason is that the MBOA is effectively optimizing the features with high convergence speed, and thus DSCNN-MBOA has good validation results with a high F1-sore rate. The combined power of CNN, modified AlexNet and attention mechanism prove advantageous in LC detection.

2) Execution time comparison results: From Fig. 7, it indicates the execution time of proposed and existing models for the number of features in a given database. As increasing the number of features, the execution time is also maximized. E.g., the DSCNN-MBOA attains a recall of 527.15s compared to the VDSNet, modified AlexNet and CNN with TL. Because the proposed model can reduce more bias in all datasets and reduce minor variance and thus the model is simple to process the LC.

3) Specificity comparison results: From Fig. 8, it indicates the recall of proposed and existing models for the number of features in a given database. As increasing the number of features, the recall is also maximized. E.g., the DSCNN-MBOA attains a recall of 89.65% compared to the VDSNet, modified AlexNet and CNN with TL. Because existing methods are simple models that are ineffective for high-dimensional datasets, they are under fitting. EASFMC has the advantage of good segmentation of cancer regions, thus increasing the classification rate of the proposed DSCNN-MBOA. Existing techniques generally perform not well when images are rotated, tilted, or otherwise strangely oriented. As a result, hybrid approaches have improved accuracy while decreasing training time. The study's findings imply that DL models can be utilized to strengthen diagnosis when compared to standard methods.
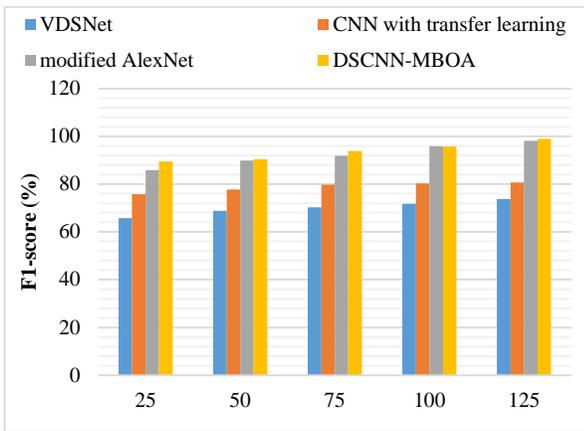
Fig. 6.   F1-score Performance Comparison.
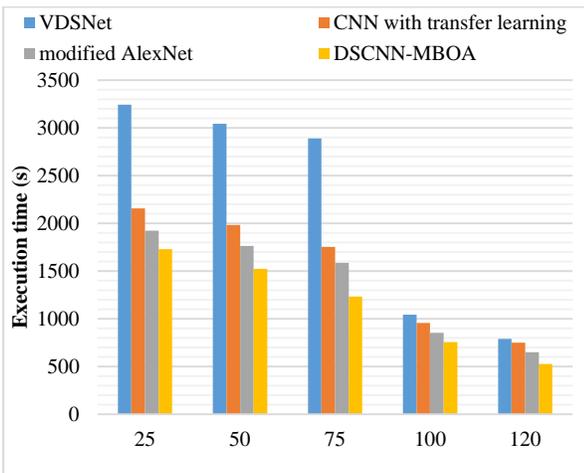
Fig. 7.   Execution Time Performance Comparison.
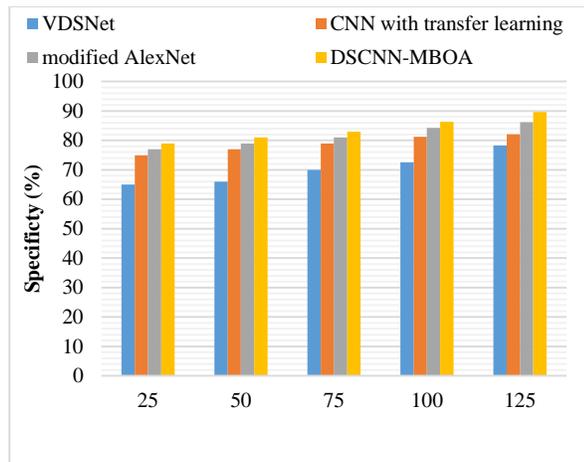
Fig. 8.   Specificity Performance Comparison.

4) Sensitivity comparison results: From Fig. 9, it gives the accuracy of proposed and existing models for the number of features in a shared database. The DSCNN-MBOA increases the accuracy and attains the sensitivity 95% when compared to VDSNet, modified AlexNet and CNN with TL. Thus the

proposed algorithm is more significant than the existing algorithms for better good validation results for predicting cancer. The proposed DSCNN-MBOA model was utterly independent of the abrupt feature changes. Thus, it could be helpful for LC n X-ray images. As can be seen from the results, the average max pooling is beneficial for the DSCNN model. Better performance can be achieved can reduce the influence of class imbalance on the training process and making the model pay more attention to classes that are difficult to recognize.
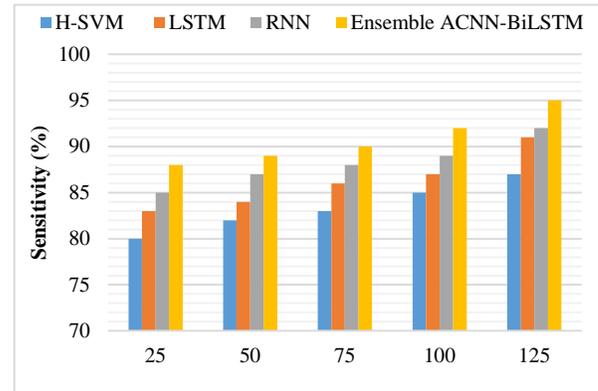
Fig. 9.   Sensitivity Performance Comparison.

V.   CONCLUSION AND FUTURE WORK

On the basis of chest X-ray images, this study presents a hybrid DL (DSCNN-MBOA) based approach for LC identification. In order to improve cancer detection performance, the phases of background segmentation, feature set extraction, feature optimization, and DSCNN-based LC classification are used. The proposed method achieves a precision of 98.45% and a time complexity of 527.15s while maintaining a tradeoff with network performance. In chest X-ray images, the proposed hybrid technique may effectively detect the cancer zone. When working with a large dataset, this research project faces a number of problems. As a result, while small datasets can generate great accuracy, they are impractical for real-world applications. Besides applying improved DL or other innovative TL algorithms for the sample, then combining GoogLeNet, AlexNet, and ResNet-152 architecture to create a hybrid algorithm in the future, this study will combine GoogLeNet, AlexNet, and ResNet-152 architecture to create a hybrid algorithm. The use of image data augmentation techniques such as color space augmentations, feature space augmentations, hyper parameter optimization, and other methods to improve the accuracy of automated chest X-ray diagnosis systems will be explored. In future research, even though the dual dataset method is successful, a more advanced deep learning method will be proposed for lung disease detection. In the first study, more datasets will be collected to increase efficacy. As is common knowledge, deep learning success is strongly influenced by the quantity of labeled data available. So this research will combine hybrid deep neural networks. A study is also planned to develop novel robust optimization based hybrid CNN-based lung segmentation with multiple datasets.

REFERENCES

[1] Siegel, R. L., Miller, K. D., Fedewa, S. A., Ahnen, D. J., Meester, R. G., Barzi, A., &Jemal, A. (2017). Colorectal cancer statistics, 2017. CA: a cancer journal for clinicians, 67(3), 177-193.

[2] Mathur, P., Sathishkumar, K., Chaturvedi, M., Das, P., Sudarshan, K. L., Santhappan, S., & ICMR-NCDIR-NCRP Investigator Group. (2020). Cancer statistics, 2020: report from national cancer registry programme, India. *JCO Global Oncology*, *6*, 1063-1075.

[3] Valente, I. R. S., Cortez, P. C., Neto, E. C., Soares, J. M., de Albuquerque, V. H. C., & Tavares, J. M. R. (2016). Automatic 3D pulmonary nodule detection in CT images: a survey. *Computer methods and programs in biomedicine*, *124*, 91-107.

[4] Yang, L., Xu, H. Y., & Wang, Y. (2020). Diagnostic and therapeutic strategies of LC patients during the outbreak of 2019 novel coronavirus disease (COVID-19). *Zhonghuazhongliuzazhi [Chinese journal of oncology]*, *42*(4), 292-295.

[5] Kadir, T., & Gleeson, F. (2018). LC prediction using machine learning and advanced imaging techniques. *Translational LC research*, *7*(3), 304.

[6] Sun, W., Zheng, B., & Qian, W. (2017). Automatic feature learning using multichannel ROI based on deep structured algorithms for computerized LC diagnosis. *Computers in biology and medicine*, *89*, 530-539.

[7] Sun, W., Zheng, B., & Qian, W. (2016, March). Computer aided LC diagnosis with DL algorithms. In *Medical imaging 2016: computer-aided diagnosis* (Vol. 9785, pp. 241-248). SPIE.

[8] NIH sample Chest X-rays Dataset Available at: https://www.kaggle.com/nih-chest-xrays/sample, Accessed 28th Jun 2020.

[9] O. Er, N. Yumusak, and F. Temurtas, "Chest diseases diagnosis using artificial neural networks," *Expert Systems with Applications*, vol. 37, no. 12, pp. 7648–7655, 2010.

[10] O. Er, C. Sertkaya, F. Temurtas, and A. C. Tanrikulu, "A comparative study on chronic obstructive pulmonary and pneumonia diseases diagnosis using neural networks and artificial immune system," *Journal of Medical Systems*, vol. 33, no. 6, pp. 485–492, 2009.

[11] S. Khobragade, A. Tiwari, C. Y. Pati, and V. Narke, "Automatic detection of major lung diseases u sing chest radiographs and classification by feed-forward artificial neural network," in Proceedings of 1st IEEE International Conference on Power Electronics. *Intelligent Control and Energy Systems* (ICPEICES-2016), pp. 1–5, Delhi, India, 2016.

[12] G. Litjens, T. Kooi, E. B. Bejnordi et al., "A survey on deep learning in medical image analysis," *Medical Image Analysis*, vol. 42, pp. 60–88, 2017.

[13] S. Albarqouni, C. Baur, F. Achilles, V. Belagiannis, S. Demirci, and N. Navab, "Aggnet: deep learning from crowds for mitosis detection in breast cancer histology images," *IEEE Transactions on Medical Imaging*, vol. 35, no. 5, pp. 1313–1321, 2016.

[14] G. E. Hinton, S. Osindero, and Y. W. Teh, "A fast learning algorithm for deep belief nets," *Neural Computation*, vol. 18, no. 7, pp. 1527–1554, 2006.

[15] H.-C. Shin, K. Roberts, L. Lu, D. Demner-Fushman, J. Yao, and R. M. Summers, "Learning to read chest X-rays: recurrent neural cascade model for automated image annotation," *Cornel University library*, 2016.

[16] Liu, C., Wang, B., Jiao, Q., & Zhu, M. (2019, June). Reducing false positives for lung nodule detection in chest X-rays using cascading CNN. In *2019 14th IEEE Conference on Industrial Electronics and Applications (ICIEA)* (pp. 1204-1207).

[17] Peng, G., Liu, L., Zeng, K., Li, T., & Nakayama, S. (2012, December). LC Detection in Chest X-Ray Images with Parallel Genetic Algorithm. In *2012 13th International Conference on Parallel and Distributed Computing,Applications and Technologies* (pp. 189-192).

[18] Ausawalaithong, W., Thirach, A., Marukatat, S., &Wilaiprasitporn, T. (2018, November). Automatic LC prediction from chest X-ray images using the DL approach. In *2018 11th Biomedical Engineering International Conference (BMEiCON)* (pp. 1-5).

[19] Yan, C., Yao, J., Li, R., Xu, Z., & Huang, J. (2018, August). Weakly supervised DL for thoracic disease classification and localization on chest x-rays. In *Proceedings of the 2018 ACM international conference on bioinformatics, computational biology, and health informatics*,pp. 103-110.

[20] Wibisono, A., Adibah, J., Priatmadji, F. S., Viderisa, N. Z., Husna, A., &Mursanto, P. (2019, November). Performance Analysis of DL Network Models of Localized Images in Chest X-ray Decision Support System. In *Proceedings of the 2019 3rd International Conference on Big Data Research* (pp. 54-59).

[21] Bhandary, A., Prabhu, G. A., Rajinikanth, V., Thanaraj, K. P., Satapathy, S. C., Robbins, D. E. & Raja, N. S. M. (2020). DL framework to detect lung abnormality–A study with chest X-Ray and lung CT scan images. *Pattern Recognition Letters*, *129*, 271-278.

[22] Bharati, S., Podder, P., &Mondal, M. R. H. (2020). Hybrid DL for detecting lung diseases from X-ray images. *Informatics in Medicine Unlocked*, *20*, 100391.

[23] Maheswari, D., &Radha, V. (2010). Noise removal in compound image using median filter. *IJCSE) International Journal on Computer Science and Engineering*, *2*(04), 1359-1362.

[24] Huang, M., Yu, W., & Zhu, D. (2012, August). An improved image segmentation algorithm based on the Otsu method. In *2012 13th ACIS International Conference on Software Engineering, Artificial Intelligence, Networking and Parallel/Distributed Computing* (pp. 135-139).

[25] Hara, K., Saito, D., &Shouno, H. (2015, July). Analysis of function of rectified linear unit used in DL. In *2015 international joint conference on neural networks (IJCNN)* (pp. 1-8).

[26] Arora, S., & Singh, S. (2019). Butterfly optimization algorithm: a novel approach for global optimization. *Soft Computing*, *23*(3), 715-734.

[27] Tubishat, M., Alswaitti, M., Mirjalili, S., Al-Garadi, M. A., & Rana, T. A. (2020). Dynamic butterfly optimization algorithm for feature selection. *IEEE Access*, *8*, 194303-194314.